Engenharia Agrícola
ISSN: 1809-4430 (online)
www.engenhariaagricola.org.br | www.scielo.br/j/eagri

Technical Paper
DOI: http://dx.doi.org/10.1590/1809-4430-Eng.Agric.v45e20230186/2025

DEVELOPMENT OF A GRAVITATIONAL AND PENDULUM SOLAR TRACKER FOR STANDALONE PHOTOVOLTAIC PANELS

Jorge A. Wissmann[1*], Carlos E. C. Nogueira[1], Marcelo M. M. Zampiva[1], Jair A. C. Siqueira[1], Doglas Bassegio[1]

[1*]Corresponding author. Universidade Estadual do Oeste do Paraná/Cascavel - PR, Brasil.
E-mail: jorge.wissmann@unioeste.br | ORCID ID: https://orcid.org/0000-0002-6099-7514

KEYWORDS

manual tracker, potential energy, analog prototype, renewable energy, pendulum control.

ABSTRACT

The contribution of photovoltaic energy has steadily increased within the energy matrix worldwide. Within this renewable energy system, optimization is there is continually pursued, which can be achieved through various approaches, including advancements in photovoltaic cell technology, impedance adjustments, inverter efficiency, collected energy storage (either on- or off-grid), cell cooling, module cleaning, and solar position tracking, which was the focus of this study. In remote areas without electrical grid access, motorized systems may not be feasible. A tracking prototype was developed whose structure is classified as chronological due to its fixed rotation, manual as it requires daily adjustment, single-axis azimuthal, and "analog" as it lacks motors, sensors, or algorithms. The results showed that the developed tracking prototype achieved a 9.69% energy production increase during the research period, with peaks of 35.51% on sunny days, and a significant efficiency improvement during the early morning and late afternoon. Statistical analysis results revealed a significant energy production difference between panels. In terms of economy, the prototype proved unviable when compared to the cost of grid electricity.

INTRODUCTION

To optimize the energy collection by photovoltaic panels, various automated solar tracking systems (solar trackers) are available, including single- (east–west orientation) and dual-axis systems (accounting for ecliptic tilt variations throughout the year with a north–south second axis). These systems are equipped with digital components (sensors and hardware) controlled by software, such as Arduino, to ensure orthogonal panel positioning relative to the direct solar radiation incidence in alignment with the sun's variable position along its elliptical trajectory (Wissmann et al., 2022).

According to Pinho & Galdino (2014), weather conditions influence the evaluation of solar irradiation periods during tracking. They also mentioned that it is common to use an alternative term, hours of full sunlight (HFS), which is defined as the number of hours during which the irradiance remains constant at 1 kW/m².

Additionally, there are several tracking system classification methods, which are typically compared with fixed systems. Seme et al. (2020) proposed a hybrid classification system that grouped different systems, including fixed and tracking systems. The latter are further classified based on their operation (active or passive), number of axes (single or dual), and tracking strategy (closed loop, open loop, or hybrid).

Katche et al. (2023) conducted a review of maximum power point tracking (MPPT) techniques in photovoltaic panel systems, classifying them into conventional, intelligent, optimized, and hybrid systems. They concluded that conventional methods are less expensive and perform better under full-sun conditions. Musa et al. (2023) reviewed single-axis time-based (chronological) solar tracking systems. They concluded that this photovoltaic technology can be used for various electrical purposes, particularly in rural areas.

[1] Universidade Estadual do Oeste do Paraná/Cascavel - PR, Brasil.

Area Editor: Juliana Lobo Paes
Received in: 12-29-2023
Accepted in: 12-5-2024

As the name suggests, chronological tracking is a time-based system that adjusts daily at a pre-defined rate. Hafez et al. (2018) stated that the variation rate depends on the type of rotation axis and the desired amplitude. The motor is controlled to rotate at a low rate of approximately 15 º/h. Pinho & Galdino (2014) also explained that during the day, a solar incidence window of approximately 12 h is observed, emphasizing that solar or angular time differs from the local standard time and corresponds to an angle of 15º in the elliptical trajectory, totaling 360º over a 24-h period.

Wissmann et al. (2022) conducted a review on solar tracking and found that, in general, the goal is to minimize the number of tracker movements to avoid making their implementation unfeasible. Tracker operation requires a certain amount of electrical energy, which may come directly or indirectly from the main photovoltaic module, thus reducing the total efficiency gain. While there is a real gain achieved by the tracking system, there is also an energy loss associated with its operation.

Olejár et al. (2015) reported 33.78% increase in electrical energy due to the implementation of single-axis tracking. They found that this gain was primarily observed at the beginning and end of the day, when the tracker's advantage over fixed systems are more evident.

Buyse (2017) recalled that Christiaan Huygens (1629–1695) invented the pendulum clock in 1656, based on the isochronism principle discovered by Galileo (1564–1642). The author also suggested that it was difficult to believe that Huygens was unaware of Galileo's idea of constructing a pendulum-regulated clock (Figure 1).

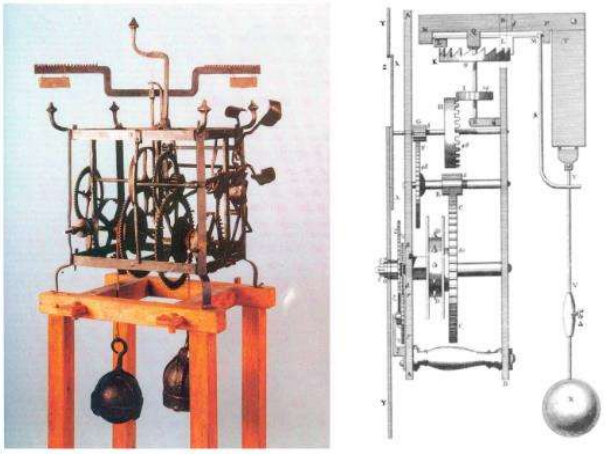

FIGURE 1. Traditional mechanical clock (left) and Huygens pendulum clock (right). Source: Buyse (2017).

Gravitational potential energy (GPE) is used in pendulum-operated clocks, where counterweights are positioned to rotate specific axes connected to the clock's internal gears. This rotational movement is regulated by the pendulum's swing, which releases potential energy in a controlled manner. A multi-gear system is employed to reduce or increase the rotational speed between axes, ultimately achieving the correct rotation of the hour, minute, and second hands.

Farooqui (2013) used a system similar to the one developed in this study (analog), but equipped with a mechanical hydraulic system and springs to rotate a solar cooker to track the Sun's position, thereby improving its efficiency.

The objective of this study was to develop and evaluate a novel solar tracker prototype. Given that the energy demand for implementing automated tracking is significant for individual photovoltaic panels (virtually rendering their implementation unfeasible), our prototype presents itself as an alternative to current tracking systems.

SUBJECT DESCRIPTION

The developed prototype is equipped with a mechanical gravitational potential system, using gears, a pendulum, and counterweights to perform daily solar tracking (east–west), similar to the mechanism of old analog clocks, a technology and principle long used to measure time and track the movement of celestial bodies, in this case, the Sun. The prototype was produced at the State University of Western Paraná (UNIOESTE) in Cascavel, Paraná, Brazil, with GNSS coordinates of -24.98912 S and -53.44927 W. This location is open, with no interference from nearby buildings, and other photovoltaic experiments were also conducted. Two identical panels were used (Figure 2), with a mounting structure featuring posts at an angle β of 36º relative to the ground.

FIGURE 2. Location of the prototype installation, both panels initially fixed, Stage 1.

In the first stage, Stage 1 (January 1–13, 2023), the two panels were compared while both were fixed (stationary). In the second stage, Stage 2 (December 13, 2023, to January 28, 2024), one of the panels was equipped with the solar tracker prototype developed in this study. For comparison, typical sunny days were used to better illustrate the radiation collection data.

During the first period, a typical sunny day, January 5, 2023, was selected as an example. Irradiance data were collected and converted into hourly power, as shown in Figure 3, where a discrepancy between Panels 1 (P1) and 2 (P2) is observed. This initial collection with both panels stationary revealed that P2 exhibited slight warping, with improved efficiency during the early day hours, but decreased efficiency toward the end of the day. With the support of P2, the developed tracker was installed during the second period.

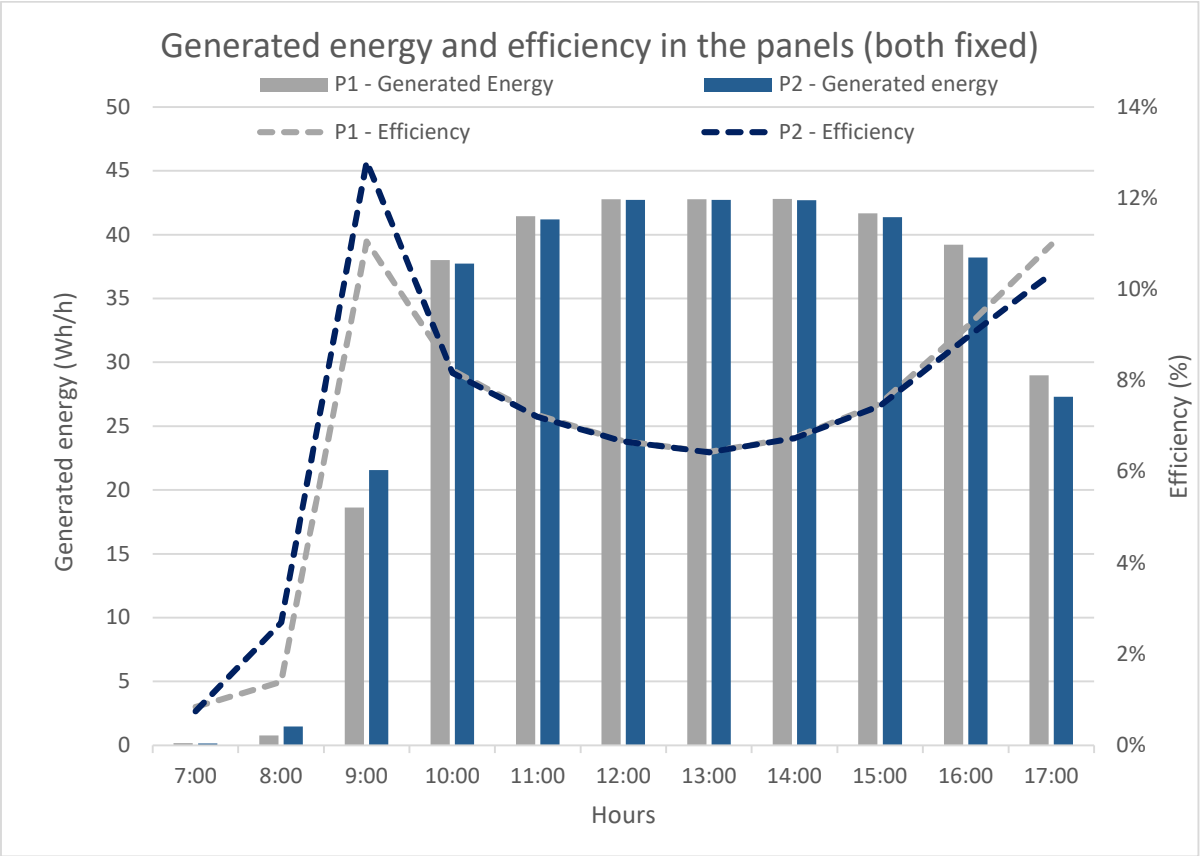

FIGURE 3. Hourly power output and efficiency readings for both fixed panels on a sunny day – Stage 1 (May 1, 2023).

A single azimuthal axis was selected for the prototype design to simplify its implementation and operation, as shown in Figure 4. The estimated weight required to generate the torque required to rotate the panel (3.2 kg) and the friction associated with the gear system to ensure continuous operation was 170 kgf. The operator must perform a daily "recharge," which involves lifting this weight using a metal lever with a tubular profile and 1 m in length. This lever is fitted with two protrusions that slot into two holes on the side of the ratchet where the chain rests, supporting the weight and counterweight. The travel of this chain was sufficient for slightly more than one full rotation per day depending on the pillar height.

FIGURE 4. Conceptualization of the azimuthal axis tracking prototype.

The following components were dimensioned using SolidWorks, a three-dimensional software: a gear set, U-shaped profile plates, bearings, protective casing, ratchet, and a step control system in the form of a horizontal pendulum (Figure 5). The prototype movement was designed for 360º rotation over 24 h (upper gear), or 15 º/h, with a weight and counterweight (gravitational) system generating the driving force for the global torque, as well as for the pendulum system (shown in red in Figure 5), which controls the step.

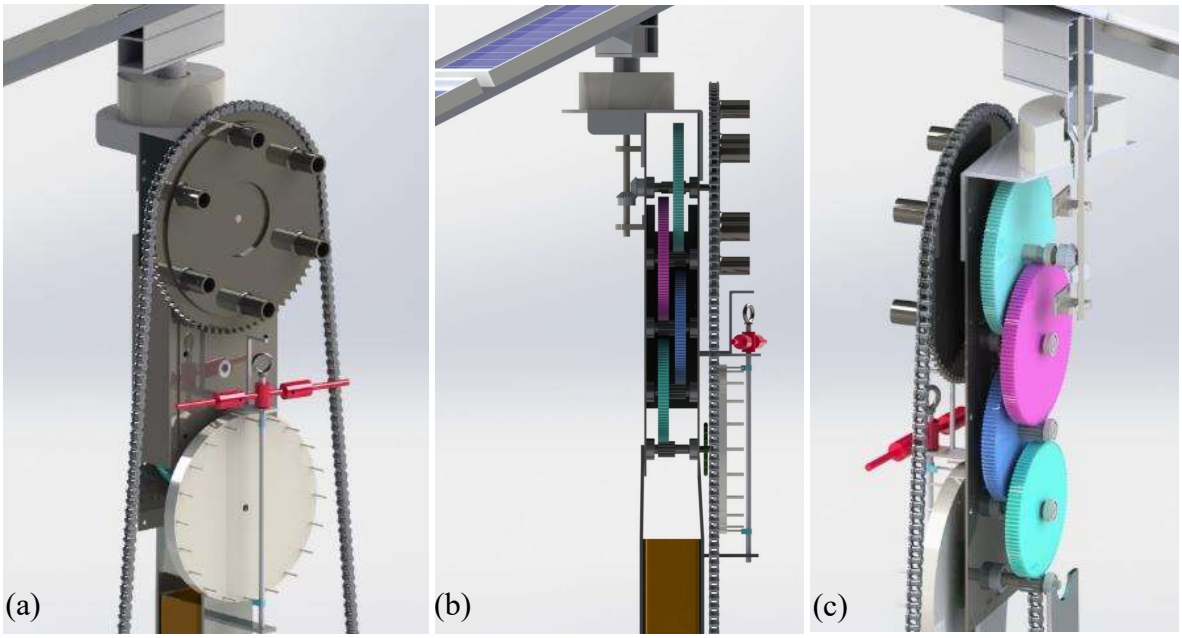

FIGURE 5. Details of the tracking prototype in 3D design software, views: (a) rear (step control), (b) side, and (c) cross-section (internal gears).

The prototype efficiency testing method was based on a direct comparison between the radiation collected by the stationary and tracking panels during Stage 2. For this, sensors, voltage- and current-reading equipment, and resistors for dissipating the generated direct current are required (Table 1).

TABLE 1. Equipment used for radiation collection.

Equipment	Brand	Model	Characteristic
Photovoltaic modules	Suntech	STP022-12/D	16.8V power
Datalogger	Campbell Scientific	CR1000	8 reading channels
Pyranometer	Kipp & Zonen	CMP3	Max radiance 2000 Wm^{-2}
Temperature sensor	Switerm	SMTJ	Nickel chromium J type
Resistors	-	helical	1000W and 8 ohms (parallel)

In this study, the installation was carried out according to the diagram shown in Figure 6, which shows a schematic of the voltage and current measurement system generated in each of the photovoltaic modules, where circles 5H and 5L represent the current reading channels, and 4H and 4L represent the voltage reading channels (HIGH and LOW, respectively).

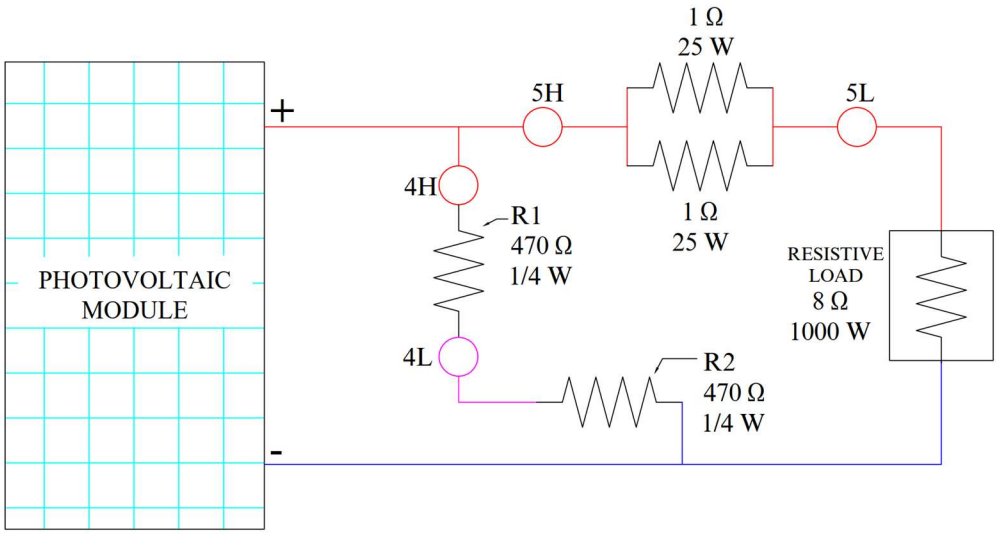

FIGURE 6. Schematic diagram for voltage and current readings of each panel.

With the tracking prototype installed, the specific variables described in Table 2 were monitored, effectively comparing the solar radiation collected by the two photovoltaic panels (namely, the stationary and tracking panels).

TABLE 2. Variables monitored in the efficiency study of the tracking prototype.

Abbreviation	Variable descriptions
Vf	Fixed module electrical voltage
If	Fixed module electric current
Vr	Electrical voltage of the module equipped with tracker
Tr	Electrical current of the module equipped with tracker
Tf	Stationary module temperature
Rs	Incident solar radiation

The panel efficiency was evaluated based on the solar radiation incident on the horizontal plane, collected by the pyranometer, but corrected for the inclined plane according to an angle of 36º and the geographical location of the experiment. The incident solar position correction equations proposed by Duffie & Beckman (2013) are as follows:

$$\delta = 23.45\ sin\left(360\frac{284+}{365}\right) \quad (1)$$

$$\theta_{z,noon} = |-\phi + \delta| \quad (2)$$

$$\omega'_s = min\begin{bmatrix} cos^{-1}(-tan\phi.tan\delta) \\ cos^{-1}(-\tan(\phi+\beta).tan\delta) \end{bmatrix} \quad (3)$$

$$\cos\omega_s = -\frac{sin\phi.sin\delta}{cos\phi.cos\delta} = -tan\phi.tan\delta \quad (4)$$

$$\bar{R}_b = \frac{\cos(\phi+\beta)cos\delta.sin\omega'_s+\left(\frac{\pi}{180}\right)\omega'_s.\sin(\phi+\beta).sin\delta}{\cos\ .cos\delta.sin\ _s+\left(\frac{\pi}{180}\right)\omega_s.\sin\ .sin\delta} \quad (5)$$

$$H_0 = \frac{24\times360\ \ sc}{\pi}\left(1+0.033cos\frac{360}{365}\right)\times\left(\cos\phi.cos\delta.sin\omega_s+\frac{\pi\omega_s}{180}sin\phi.sin\delta\right) \quad (6)$$

$$\bar{H}_T = \frac{\bar{H}}{\bar{H}_0} \quad (7)$$

$$\frac{\bar{H}_d}{\bar{H}} = 1.391 - 3.560\bar{H}_T + 4.189\overline{K_T}^2 - 2.137\overline{K_T}^3 \quad (8)$$

$$\frac{\bar{H}_d}{\bar{H}} = 1.311 - 3.022\overline{K_T} + 3.427\overline{K_T}^2 - 1.821\overline{K_T}^3 \quad (9)$$

$$\bar{R} = \frac{\bar{H}_T}{\bar{H}} = \left(1-\frac{\bar{H}_d}{\bar{H}}\right)\bar{R}_b + \frac{\bar{H}_d}{\bar{H}}\left(\frac{1+cos\beta}{2}\right) + \rho_g\left(\frac{1-cos}{2}\right) \quad (10)$$

Where:

δ: solar declination for a specific day [°];

θ_z: angle of incidence of solar radiation measured from the zenith [°];

ϕ: local latitude [°];

β: tilt angle of the plane relative to the horizontal surface plane [°];

G_{sc}: solar constant with a value of 1.367 W/m²;

H: daily solar irradiation on a horizontal plane on the Earth's surface [Wh/m²];

Ho: monthly average daily extraterrestrial radiation on a horizontal plane;

$\bar{H}$: monthly average solar irradiation on the horizontal plane of the Earth's surface [Wh/m²];

H_o: monthly average extraterrestrial solar irradiation at the top of the atmosphere on a theoretical horizontal plane [Wh/m²];

$\bar{H}_d$: monthly average diffuse solar irradiation [Wh/m²];

$\bar{H}_T$: global solar irradiation on an inclined plane [Wh/m²/day];

K_T: average clearness index;

$\bar{K}_T$: monthly average atmospheric clarity or transparency index;

n: date measured by ordinal number from 1 to 365;

$\bar{R}$: ratio between the average daily beam radiation on the inclined surface and the horizontal surface;

$\bar{K}_b$: proportion of the average daily beam radiation on the inclined surface and the horizontal surface on a monthly basis;

ω_s: sunset hour angle [°];

ω'_s: sunset hour angle for an inclined surface [°].

Statistical analyses were conducted in RStudio using the R programming language. The economic analysis was performed using the levelized cost of energy (LCOE) and economic variables listed in Table 3.

TABLE 3. Parameters used for the economic evaluation.

Parameters	Value	Unit
Fixed system maintenance	1%	Per year
Mobile system maintenance	5%	Per year
Inflation	4%	Per year
Minimum attractiveness rate	6%	Per year
Panel power	66	W
Panel area	0.68	m^2
Hours of full sunlight (HFS) fixed module	4.60	h/day
Hours of full sunshine (HFS) mobile module	5.33	h/day
Number of days collected	47	Days
Panel performance rate	80%	-
Energy depreciation of panels	0.8%	Per year

The solar tracker prototype for P2 was constructed according to the aforementioned design, initially with four internal gears made of nylon, with reductions of 125 to 120 and 110 to 100, along with five metal pinions, each with 14 teeth. This setup resulted in one 360º rotation every 24 h (0.000693788 rpm or 86,400 s) for the upper gear and one rotation every 20 s (3 rpm) for the lower gear, which controlled the time (or step). After assembly and initial tests, several part adjustments and resizing were made, such as replacing the upper gear with a metal one, adjusting the scale of the step control anchor, installing a new metal pillar for mounting (orange), using a larger-diameter ratchet, and creating a larger external protective casing against weather conditions, resulting in the final prototype version, which began operating continuously once the weight system was loaded (Figures 7 and 8).

FIGURE 7. P1 - stationary (left) and prototype details for P2 - trackable (right).

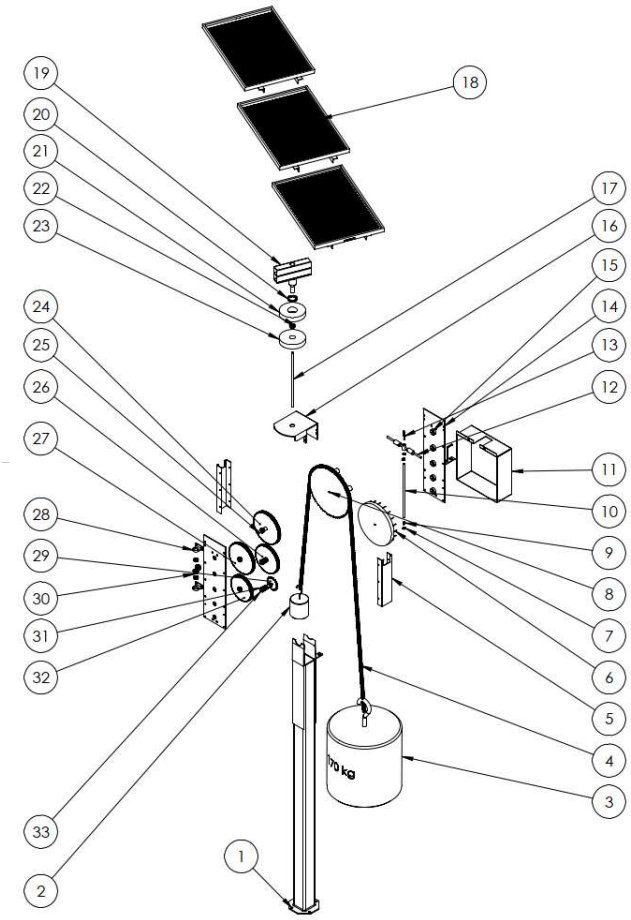

N.	PART NUMBER	QUANT.
1	PILLAR	1
2	COUNTERWEIGHT	1
3	WEIGHT	1
4	CHAIN	1
5	U - BEAM	2
6	NYLON WHEEL	1
7	SKF - 618-8 - 12,SI,NC,12_68	2
8	CHAIN WHEEL/ SPROCKET	1
9	KEY	2
10	OSCILLATING SHAFT	1
11	OSCILLATING BERING	1
12	OSCILLATING ARM	1
13	EYEBOLT AI 18.15_TYPE2 0.25X2.22-N-0.75	1
14	SIDE PLATE	1
15	BEARING ROLLER 6000	10
16	TOP PLATE	1
17	PANEL AXLE	1
18	SOLAR PANEL 22W	3
19	ROTATING BASE	1
20	SKF - 61808 - 32,SI,NC,32_68	1
21	UPPER NYLON WHEEL	1
22	SKF - 61804 - 18,SI,NC,18_68	1
23	UPPER NYLON WHEEL 2	1
24	GEAR 125 TEETH	1
25	OUTPUT SHAFT	1
26	GEAR 110 TEETH	1
27	GEAR 120 TEETH	1
28	BEARING SUPPORT 6200	2
29	CHAIN GEAR 18 TEETH	1
30	CONICAL GEAR	2
31	RADIAL BALL BEARING_68_SKF(SKF - 6000 - 8,SI,NC,8_68)	4
32	GEAR 100 TEETH	1
33	GEAR 14 TEETH MODULE 1,5 LONG	1

FIGURE 8. Exploded view of the Prototype.

Then, P2 equipped with the prototype was positioned daily towards the east at sunrise, completing a 180º azimuthal rotation shortly before sunset, thus tracking its elliptical trajectory.

The data show that for a typical sunny day, taking January 10, 2024, as an example, with P2 equipped with the developed tracker (prototype), an additional total gain of 9.69% in terms of energy generation was achieved through solar position (elliptical) tracking on almost all days during the period, reaching peaks of 35% on sunny days, as shown in Figure 9.

For the coordinates near the experimental site, Debastiani et al. (2022) found an average gain of 20.1%, which, according to Berwanger (2019), represents only 5% of the average additional energy generated, despite a peak generation of up to 30% on sunny days and less than 15% on rainy and cloudy days. Additionally, Sousa et al. (2022) reported that the tested solar tracker exhibited a net gain of 22.81% and 10.64%, respectively. According to Júnior et al. (2020), the gains ranged between 16% and 19% on sunny and partially cloudy days, respectively.

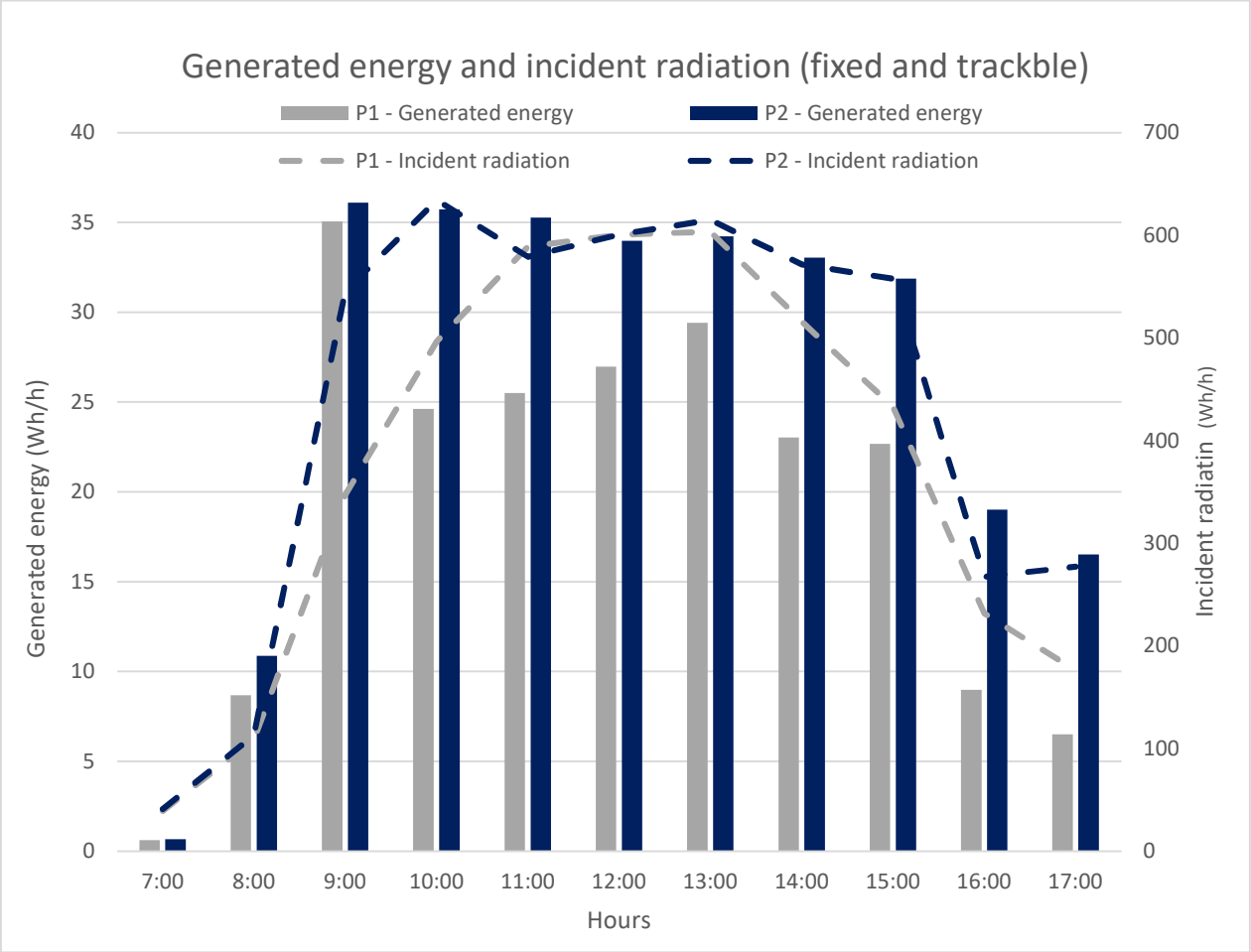

FIGURE 9. Hourly power and radiation incident on the panels on a sunny day – Stage 2 (January 10, 2024).

Applying the corrections for incident radiation to the inclined plane proposed by Duffie & Beckman (2013), it was possible to measure the panel efficiency for both the stationary (Table 4), where the azimuthal surface angle was fixed at 180°, and variable-angle (according to the time of day) systems (Table 5).

TABLE 4. Radiation collection efficiency for P1 – stationary (γs =180°).

Hour	Surface azimuthal angle (degrees)	Solar radiation read in the horizontal plane (W/m^2)	Incident solar radiation on the inclined plane (W/m^2)	Incident solar radiation on module 1 - fixed (Wh/h)	Energy generated in module 1 - fixed (Wh/h)	Mean efficiency of module 1 - fixed (%)
7:00	180	63.08	57.66	39.21	0.60	1.54
8:00	180	174.60	159.92	108.75	8.68	7.98
9:00	180	672.50	510.60	347.21	35.06	10.10
10:00	180	896.00	730.39	496.66	24.62	4.96
11:00	180	1022.00	866.18	589.00	25.51	4.33
12:00	180	1023.00	883.58	600.83	26.97	4.49
13:00	180	1028.00	887.64	603.60	29.42	4.87
14:00	180	885.00	758.60	515.85	23.03	4.46
15:00	180	765.90	636.19	432.61	22.67	5.24
16:00	180	383.00	340.96	231.85	8.97	3.87
17:00	180	321.90	258.74	175.94	6.49	3.69
	Total	7234.98	6090.45	4141.51	212.01	
					Mean	5.05

TABLE 5. Radiation collection efficiency for P2 – traceable (γs = variable).

Hour	Surface azimuthal angle (degrees)	Solar radiation read in the horizontal plane (W/m^2)	Incident solar radiation on the inclined plane (W/m^2)	Incident solar radiation on module 2 - mobile (Wh/h)	Energy generated in module 2 - mobile corrected (Wh/h)	Mean efficiency of module 2 - mobile (%)
7:00	-105	63.08	60.32	41.02	0.66	1.61
8:00	-120	174.60	166.48	113.21	10.88	9.61
9:00	-135	672.50	802.18	545.48	36.10	6.62
10:00	-150	896.00	932.97	634.42	35.73	5.63
11:00	-165	1022.00	851.47	579.00	35.27	6.09
12:00	180	1023.00	883.58	600.83	33.98	5.66
13:00	165	1028.00	904.29	614.92	34.22	5.57
14:00	150	885.00	840.93	571.83	33.03	5.78
15:00	135	765.90	820.10	557.67	31.88	5.72
16:00	120	383.00	393.13	267.33	19.01	7.11
17:00	105	321.90	407.72	277.25	16.52	5.96
	Total	7234.98	7063.17	4802.95	287.29	
					Mean	5.94

The total energy generated by P1 and P2 was 212.01 and 287.29 Wh/h, respectively, an increase of 75.28 Wh/h. The average radiation collection efficiency was 5.05% and 5.94% for the stationary and tracking panels, with the latter exhibiting better efficiency.

The efficiency of both modules is shown in Figure 10. As can be seen, there are two efficiency peaks in the early hours at 8:00 AM and 9:00 AM, with 9.6% and 10.1% for the tracking and stationary panels, respectively.

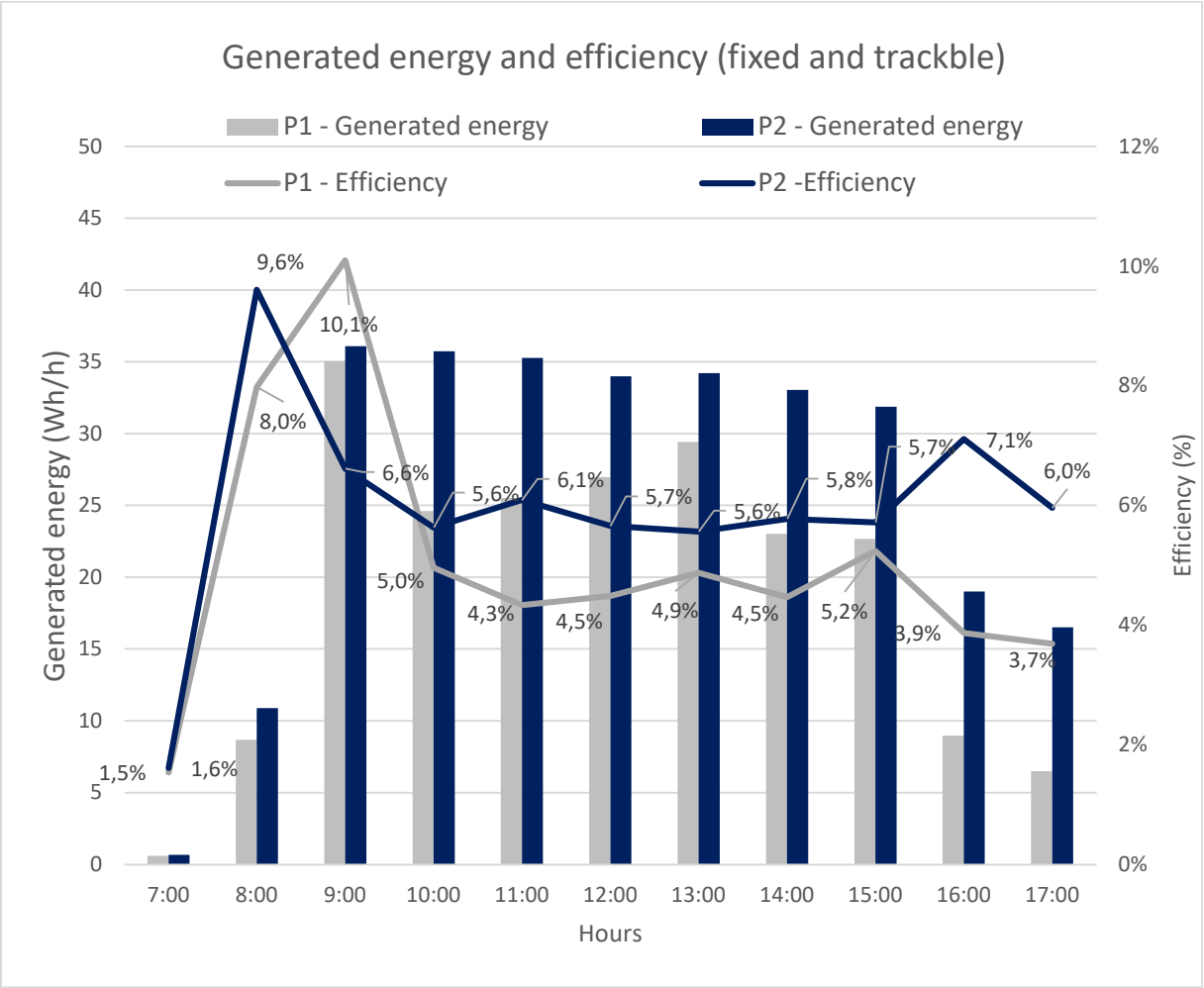

FIGURE 10. Hourly comparison of stationary and trackable panel efficiency – Stage 2 (January 10, 2024).

Debastiani et al. (2022) stated that this is the time of the day when the panels are still "cold" (Figure 11). This is also the time when the user performs the weight "recharge" and repositions the tracking panel, directing it towards the rising sun. At the end of the afternoon, a better radiation collection efficiency was observed for the panel equipped with the tracker.

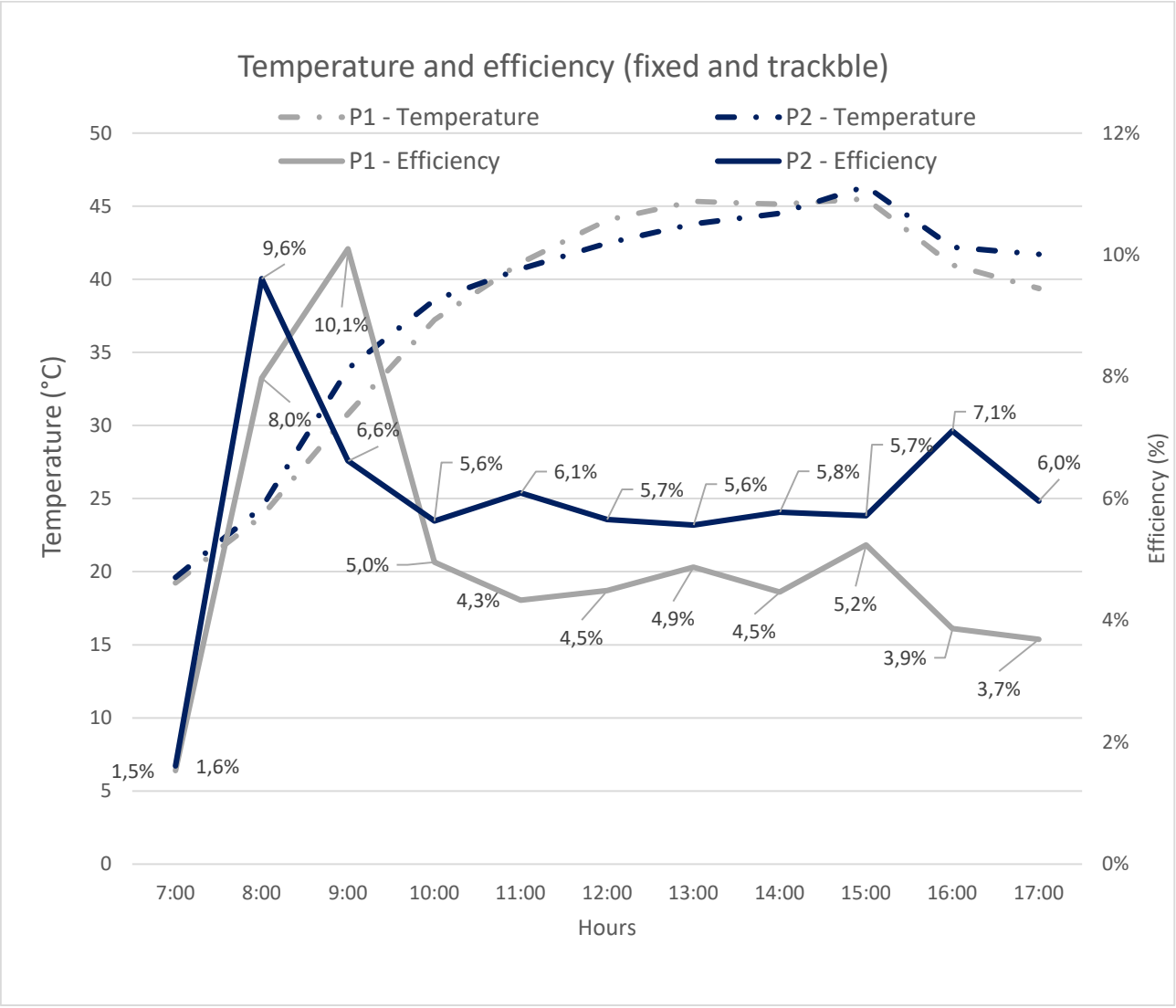

FIGURE 11. Hourly comparison of efficiency and temperature, steady-state and traceable – Stage 2 (January 10, 2024).

This slight efficiency improvement for the panel equipped with the tracker in the late afternoon can be attributed to a decrease in the temperature of the panels combined with the fact that it is oriented perpendicular to the solar rays.

The statistical analysis was performed on the radiation data for Stage 2, where some days were selected as sunny ("yes sun") and others as cloudy/rainy ("no sun"). These were selected as follows: sunny days: December 13, 15, 16, 17, 26, 27, 28, 30, 2023, and January 24, 2024; cloudy or rainy days: December 20, 23, 24, 25, 2023, and January 12, 15, 20, and 22, 2024. Descriptive statistics, such as mean, standard deviation, scatter plots, histograms, and boxplots, were developed to compare the results (Figure 12). Additionally, a T-Student test for mean comparison was used to assess whether there was a significant mean difference between the panels. To perform this test, the normality condition was investigated using the Shapiro-Wilk test. All inferences were made at the 5% significance level.

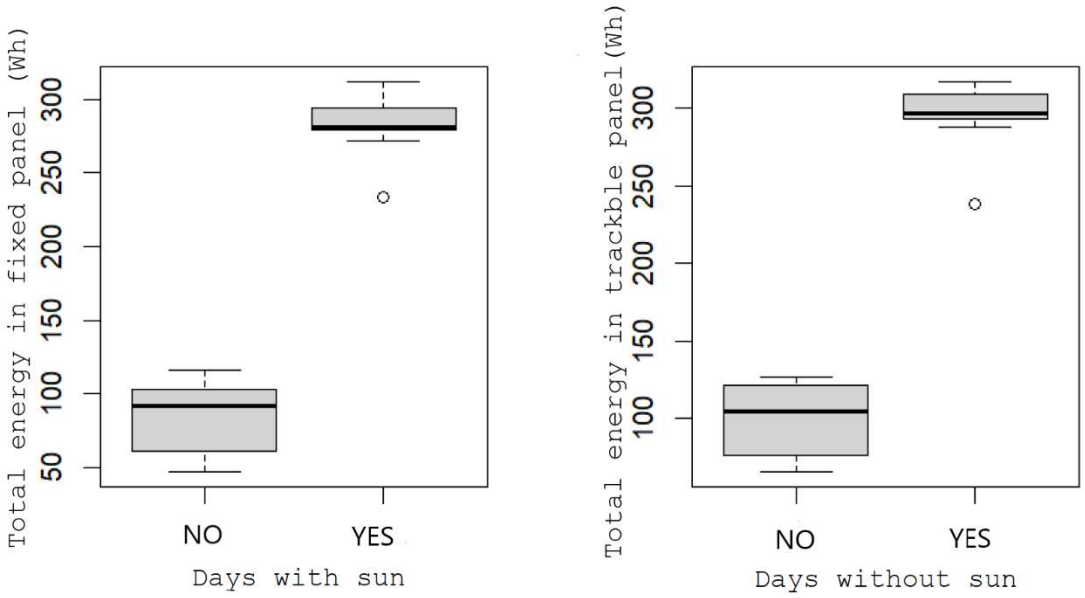

FIGURE 12. Box plots for P1 and P2 ("YES" and "NO" sun).

Subsequently, a box plot was created to assess the energy difference between panels, as shown in Figure 13 (with a mean difference of -13.14Wh), and a hypothesis test was conducted with a 5% significance level. The result was t = -6.637 with a p-value of < 0.01. Therefore, there is evidence to reject the null hypothesis that the average production between panels is equal, meaning that the fixed panel produced a significantly lower average result than the tracking panel.

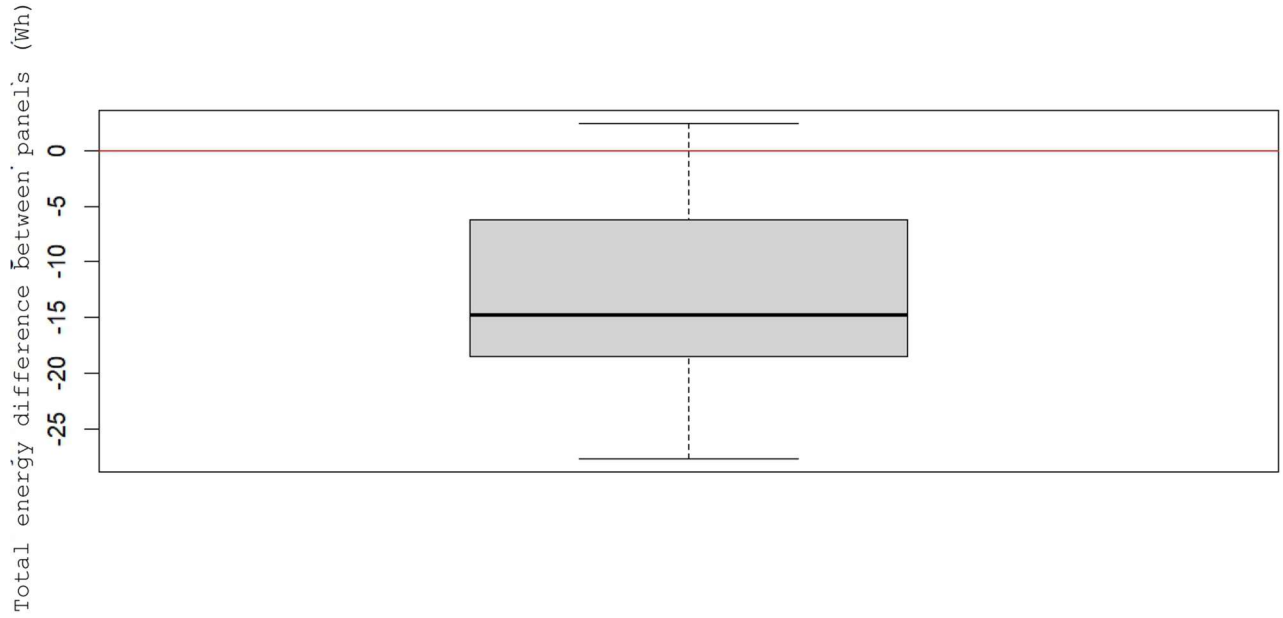

FIGURE 13. Total energy difference between panels, box plot.

For the economic evaluation, the total value for the prototype construction in its final version was used (R$ 4,574.61), along with the average HFS for each panel (fixed and tracking), comparing four possible scenarios for their LCOE:

1. Using the fixed solar panel employed in this study. The LCOE of the energy generated is R$ 0.96/kWh.
2. Using the new fixed solar panel with the same power (which produces slightly higher generation than the panel used in this study). The LCOE of the energy generated is R$ 0.79/kWh.
3. Using the solar panel with the developed tracking system. The LCOE of the generated energy is R$ 10.94/kWh.
4. Using the new solar panel with the same power with the developed tracking system. The LCOE of the generated energy is R$ 8.56/kWh.

Based on these results, it was found that the new fixed solar panel was more economically viable as it showed the lowest LCOE, whereas the solar panel with the developed tracking system exhibited the highest LCOE.

CONCLUSIONS

The main conclusions of this study can be summarized as follows.

1. The developed prototype proved to be functional for solar tracking when used with an isolated photovoltaic panel, showing an increase of 9.69% in terms of the energy generated during the analyzed period, reaching up to 35% on a sunny day. Owing to the movement of the trackable panel (provided by the developed prototype), there was an 8.4% improvement in the radiation collection efficiency.

2. The developed prototype is classified as chronological and manual, as it operates at a predefined rate and requires "recharging," with a single azimuthal axis and an "analog" strategy, as it does not rely on algorithms or sensors. The fine adjustments of the horizontal pendulum arms proved satisfactory and sensitive and achieved a rotation close to the ideal 15°/h found in the literature.

3. Statistically, the production values between the fixed and mobile panels showed a significant difference at a 5% significance level.

4. In terms of economy, the developed tracker was not attractive in the simulated scenarios compared with the cost of energy supplied by the local grid; however, it could be advantageous in remote locations.

REFERENCES

Berwanger, D. (2019). *Desenvolvimento de um sistema fotovoltaico com rastreador solar de um eixo instalado em uma propriedade rural conectado à rede*. [Dissertação de Mestrado, Universidade Estadual do Oeste do Paraná].

Buyse, F. A. (2017). Galileo Galilei, Holland and the pendulum clock. *O que nos faz pensar*, *26*(41).

Debastiani, G., Nogueira, C. E. C., Acorci, J. M., Siqueira, J. A. C., Silveira, V. F., & de Souza, S. N. M. (2022). Comparação do impacto da temperatura no desempenho de módulos fotovoltaicos estáticos e com sistemas de rastreamento solar (LO, LO+ NS). *Research, Society and Development*, *11*(4), e12311427220-e12311427220. https://doi.org/10.33448/rsd-v11i4.27220

Duffie, J. A., Beckman, W. A., & Blair, N. (2020). *Solar engineering of thermal processes, photovoltaics and wind*. John Wiley & Sons.

Farooqui, S. Z. (2013). A gravity based tracking system for box type solar cookers. *Solar Energy*, *92*, 62–68. https://doi.org/10.1016/j.solener.2013.02.024

Hafez, A. Z., Yousef, A. M., & Harag, N. M. (2018). Solar tracking systems: Technologies and trackers drive types–A review. *Renewable and Sustainable Energy Reviews*, *91*, 754-782. https://doi.org/10.1016/j.rser.2018.03.094

Júnior, A., Silva, L., Santos, M., Silva, M. (2020). Rastreador solar e comparação de eficiência na geração fotovoltaica. *Revista Científica Multidisciplinar Núcleo do Conhecimento*, *13*(8) 44–62.

Katche, M. L., Makokha, A. B., Zachary, S. O., & Adaramola, M. S. (2023). A comprehensive review of maximum power point tracking (mppt) techniques used in solar pv systems. *Energies*, *16*(5), 2206. https://doi.org/10.3390/en16052206

Musa, A., Alozie, E., Suleiman, S. A., Ojo, J. A., & Imoize, A. L. (2023). A review of time-based solar photovoltaic tracking systems. *Information*, *14*(4), 211. https://doi.org/10.3390/info14040211

Olejár, M., Cviklovič, V., Hrubý, D., & Lukáč, O. (2015). Autonomous control of biaxial tracking photovoltaic system. *Agriculture Journals,* 61, 48–52. https://doi.org/10.17221/29/2015-RAE

Tavares, J., & Galdino, M. (2014). Manual de engenharia para sistemas fotovoltaicos. *Rio de Janeiro: CEPEL-CRESESB*.

Seme, S., Štumberger, B., Hadžiselimović, M., & Sredenšek, K. (2020). Solar photovoltaic tracking systems for electricity generation: A review. *Energies*, *13*(16), 4224. https://doi.org/10.3390/en13164224

Sousa, M. D., de Abreu, W. G., & Alves, J. L. S. (2022). Desenvolvimento e análise do ganho energético líquido de um rastreador solar de eixo único conectado à rede elétrica. *Revista de Engenharia e Tecnologia*, *14*(2), 253–264.

Wissmann, J. A., Toscan, A. F., Lenz, M. L., Nogueira, C. E. C., & Siqueira, J. A. C. (2022). Revisão do rastreamento solar para sistemas fotovoltaicos. *Almanaque Multidisciplinar de Pesquisa*, *9*(1), 85–102. https://orcid.org/0000-0002-6099-7514